Elemental effects on the oxidation of refractory compositionally complex alloys

Kai-Chi Lo, Hideyuki Murakami, Uwe Glatzel, Jien-Wei Yeh, Stéphane Gorsse, An-Chou Yeh

▶ **To cite this version:**

Kai-Chi Lo, Hideyuki Murakami, Uwe Glatzel, Jien-Wei Yeh, Stéphane Gorsse, et al.. Elemental effects on the oxidation of refractory compositionally complex alloys. International Journal of Refractory Metals and Hard Materials, 2022, 108, pp.105918. 10.1016/j.ijrmhm.2022.105918 . hal-03719376

HAL Id: hal-03719376
https://hal.science/hal-03719376

Submitted on 11 Jul 2022

HAL is a multi-disciplinary open access archive for the deposit and dissemination of scientific research documents, whether they are published or not. The documents may come from teaching and research institutions in France or abroad, or from public or private research centers.

L'archive ouverte pluridisciplinaire **HAL**, est destinée au dépôt et à la diffusion de documents scientifiques de niveau recherche, publiés ou non, émanant des établissements d'enseignement et de recherche français ou étrangers, des laboratoires publics ou privés.

Elemental Effects on the Oxidation of Refractory Compositionally Complex Alloys

Kai-Chi Lo[a, b*], Hideyuki Murakami[c, d**], Uwe Glatzel[e], Jien-Wei Yeh[a, b], Stéphane Gorsse[f], An-Chou Yeh[a, b***]

[a] Department of Materials Science and Engineering, National Tsing Hua University, 101, Sec. 2, Kuang-Fu Road, Hsinchu, 300044, Taiwan, R. O. C.

[b] High Entropy Materials Center, National Tsing Hua University, 101, Sec. 2, Kuang-Fu Road, Hsinchu, 300044, Taiwan, R. O. C.

[c] Research Center for Structural Materials, National Institute for Materials Science, 1-2-1 Sengen, Tsukuba, 305-0047, Japan.

[d] Department of Nanoscience and Nanoengineering, Waseda University, 3-4-1 Okubo, Shinjuku Tokyo, 169-8555, Japan.

[e] Metals and Alloys, University of Bayreuth, Prof.-Rüdiger-Bormann-Str. 1, 95447, Bayreuth, Germany

[f] Univ. Bordeaux, CNRS, Bordeaux INP, ICMCB, UMR 5026, F-33600 Pessac, France

*Corresponding author: kaichi.lo@mx.nthu.edu.tw

**Corresponding author: MURAKAMI.Hideyuki@nims.go.jp

***Corresponding author: yehac@mx.nthu.edu.tw

Abstract

The oxidation of refractory compositionally complex alloys (RCCAs) is one of the most critical subjects for their high temperature applications. In this work, several RCCAs were systematically designed and isothermally oxidised at 1000 ˚C for up to 24 hours; the elemental effects of Al, Cr, Mo, Nb Ta, Ti, V, and Zr on the oxidation of the RCCAs were studied. It was found that Al, Cr, Ti could enhance the oxidation resistance of the RCCAs by promoting the formation of rutile-type $AlTaO_4$, $CrTaO_4$, and their related oxides, while Zr and V formed non-protective oxides such as $Nb_2Zr_6O_{17}$, $Ta_2Zr_6O_{17}$, $ZrTiO_4$, and VTa_9O_{25}, resulting in severe internal oxidation. Mo appeared to be effective in suppressing internal oxidation, but it could form non-protective $MoTiTa_8O_{25}$. Ta was slightly more beneficial than Nb for reducing the oxidation mass gain. This study provides insights on the elemental effects on the oxidation and guidelines for improving the oxidation resistance of RCCAs.

Keywords: Refractory alloys; Compositionally complex alloys; Oxidation.

1. Introduction

The development of materials for turbine engine is crucial for reducing fossil fuel consumption and global warming, since the increase in operation temperature of turbine engine can enhance its efficiency, potential materials with higher temperature capability than that of superalloys are intensively studied. Nowadays, Ni-based superalloys are widely used in the hottest sections of a gas turbine owing to their outstanding mechanical properties and surface stability. However, the temperature capability of the Ni-based superalloys has reached its limit due to the melting point of the solvent element Ni, which is 1455 ˚C. Therefore, developing new alloys with even higher melting points than Ni-based superalloys is important. Recently, RCCAs have been proposed as potential candidates for advanced high temperature applications. By combining multiple refractory elements, such as W, Ta, Mo, Nb, etc., in similar atomic ratio, RCCAs can exhibit extraordinary strength at extremely high temperature [1-7]. Although the high temperature strength of RCCAs is promising, they show poor environmental resistance in general owing to the inability to form a protective oxide scale at high temperature. While an advanced Ni-based superalloy containing Al content as low as 8.7 at% could possess excellent surface stability by forming a protective Al_2O_3 scale [8-12], RCCAs do not show such property even with 20 at% of Al content [13-27]. One of the latest developments in enhancing the oxidation resistance of RCCAs is attributed to the formation of $CrTaO_4$-based oxide scale, which has been studied at the temperature range of 900 to 1500 ˚C and up to 200 hours [20, 21, 23, 24, 28]; the formation of continuous $CrTaO_4$-based oxide scale could decrease oxidation mass gain [21, 23], but the substrate beneath it still shows certain degree of internal oxidation, which is not observed in the Al_2O_3-forming substrate [10, 11, 29-31]. Detailed examination on the internally oxidised region in the $CrTaO_4$-based-oxide-forming substrate shows strong presence of nitrides in addition to oxides [20, 21, 23, 24], indicating such oxide scale might not stop nitrogen intake and thus the nitridation of the substrate, which usually leads to its embrittlement [32]. For an advanced Ni-based superalloy, the formation of a protective Al_2O_3 scale can be achieved by means of alloying, such as adding Al, Cr, and Si [33-36]. While the alloying strategy for tuning the surface stability of Ni-based superalloys have already been well-established, the alloying effects on oxidation behaviour for RCCAs is still scarce. In this study, the oxidation behaviours of several RCCAs have been designed and analysed with respect to compositions and thermodynamic simulation. The aim of this study is to provide an understanding on the compositional effects on the oxidation of RCCAs and guidelines for designing oxidation-resistant RCCAs.

2. Material and methods

2.1 *Alloy design*

To have an overview of alloying strategy, the oxidation mass gain curves based on literature data of several representative RCCAs and a Ni-based superalloy CMSX-4 at 1000 ˚C were plotted and shown in Figure 1(a) [14, 16, 19, 20, 25, 26, 37-39]. The oxidation mass gain curves of RCCAs with short testing duration [25, 38] or microalloying [18, 40] were not included. According to composition and mass gain, these RCCAs could be divided into 3 groups: RCCAs with only Zr and other non-protective-oxide-forming elements (black lines), RCCAs with both Al and Zr (red lines), and RCCAs with Al but no Zr (blue lines).

The general trends deduced from Figure 1(a) indicate that the Al-bearing RCCAs have reduced oxidation mass gain, while Zr-bearing RCCAs have increased oxidation mass gain. In order to further elucidate the compositional effects of individual elements on the oxidation behaviour of RCCAs, new compositions were designed based on quasi-binary technique in this work: Al content was fixed at 20 at%, while the rest of the components were selected refractory elements combined in equi-molar ratio. The Al content was specifically controlled since it was considered the reference element for the formation of Al_2O_3. The deduction of compositional effects for a specific element was done by adding or removing that element from a mother composition, then comparing the results of these two alloys. Figure 1(b) shows the compositions and designations of the new alloys. NbTaTiZr was the base alloy since this composition contains frequently used elements for RCCAs [7, 41-46]. Additionally, Al, Cr, Mo, V were selected since these elements are commonly used for enhancing either the oxidation resistance [45-48] or mechanical properties [2, 4, 5, 41, 43, 44, 48-50] of RCCAs. New compositions that were investigated in order to elucidate elemental effects could be categorized into Group A, Group B and Group C.

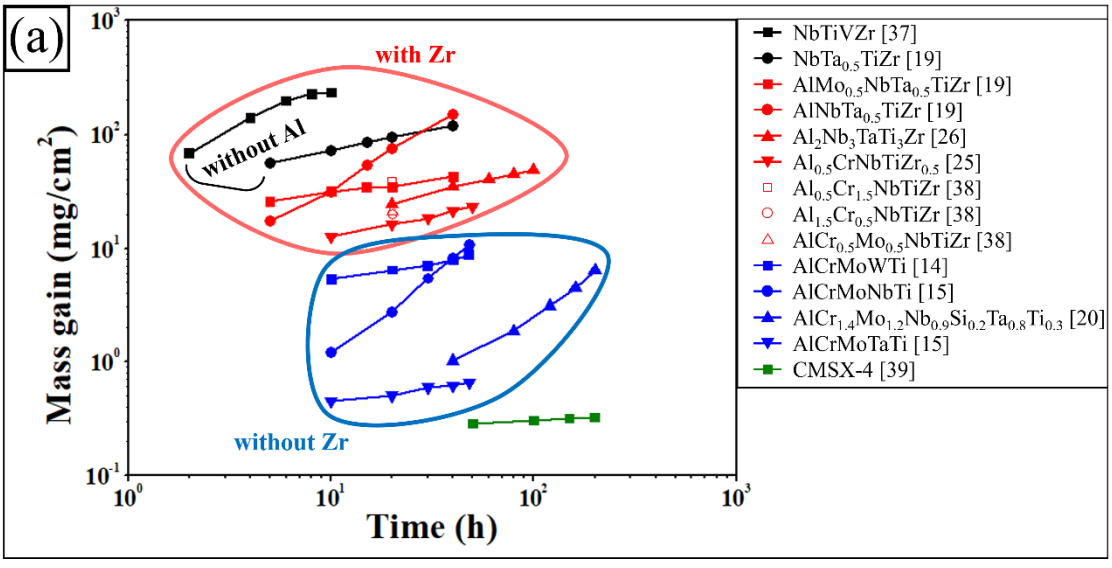

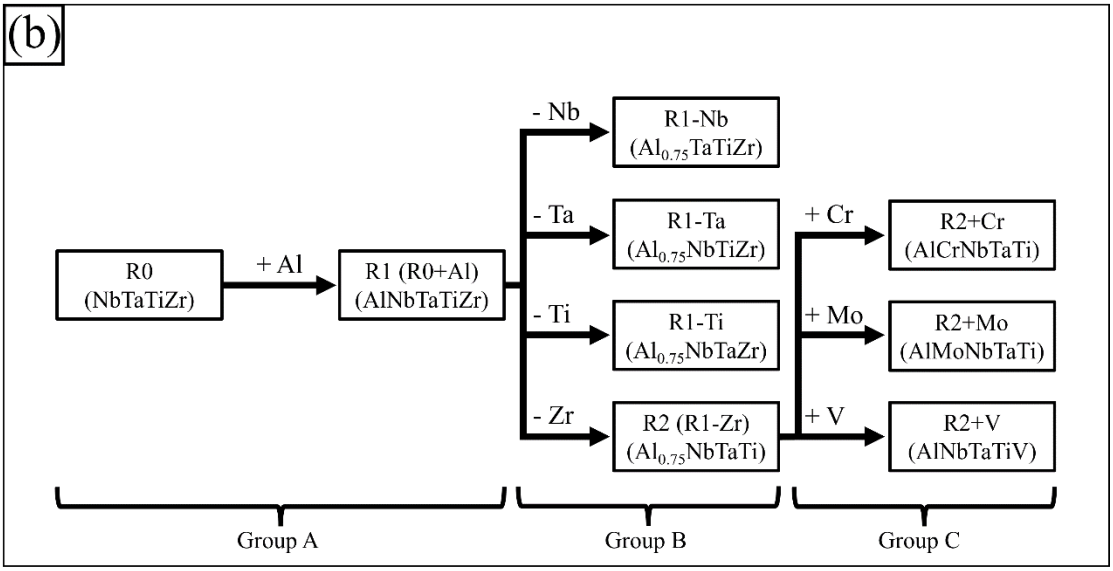

Figure 1 (a) The oxidation mass gain curves or the terminal oxidation mass gain of the selected RCCAs reported in the literature and (b) the flow chart for the design of the studied RCCAs in this work.

2.2 *Experimental procedures*

The ingots of the alloys of interest shown in Figure 1(b) were prepared by arc-melting high purity elements (> 99.9 wt%) under Ti-gettered pure argon atmosphere on a water-cooled copper hearth according to their nominal compositions. The as-cast compositions of the ingots are listed in Table 1. Each button-shaped, 20-gram ingot was flipped and re-melted 4 times to ensure the chemical homogeneity. The ingots had shiny surfaces and showed no sign of oxidation after the melting process. The ingots were subsequently electric-discharge-machined into 6 × 5 × 5 mm blocks of specimens. The top surfaces of all specimens were ground with #1200 SiC abrasive paper prior to any subsequent tests. Isothermal oxidation was performed with a muffle furnace at 1000 ˚C for various duration. The specimens were spaced 10 mm apart from each other in an Al_2O_3 boat crucible and positioned into the furnace after the furnace interior was heated to 1000 ˚C and furnace-cooled to ambient temperature upon reaching the desired testing duration. At least 2 specimens were used per alloy for the isothermal oxidation test to ensure the repeatability of the testing results. Here, 2-hour isothermal oxidation was mainly for observation on the cross-sectional microstructure, while 24-hour isothermal oxidation was mainly for X-ray diffraction (XRD) of the oxidised specimens, which was carried out with Bruker D2 Phaser equipped with Cu target. Goniometer scanning was performed between $2\theta = 20^\circ \sim 100^\circ$ with a scanning rate of 5.7˚ per minute. The oxide scales of the specimens were either ground into fine powder (for specimens oxidised for 24 hours) or kept on the top surfaces of the specimens (for specimens oxidised for 2 hours) for XRD analysis.

Thermogravimetric analysis (TGA) was also carried out in flowing dry air at 1000 ˚C for up to 2 hours with SETARAM TAG 24- 18S simultaneous symmetrical thermoanalyser to investigate the oxidation kinetics of the studied RCCAs. Specimens for TGA had dimensions of 6 × 3 × 2 mm^3 with each surface ground with #1200 SiC abrasive paper. Each specimen was carefully placed in a micro Al_2O_3 cylindrical crucible to minimize its contact with the crucible, then the crucible with specimen was hung by a Pt wire vertically. The mass gain of the specimen was recorded automatically every 0.02 minute up to 2 hours with an accuracy of 0.023 μg. Each tested TGA specimen was compared with that of isothermal oxidation tests to ensure the consistency between the results. The mass of the tested TGA specimen itself and the total mass of the tested TGA specimen with the crucible were also measured to evaluate the spallation of the specimens. The specimens were polished with 0.02 μm colloidal silica prior to metallographic observation with a JEOL-JSM 7610F scanning electron microscope (SEM) equipped with back-scattered electron (BSE) and energy-dispersive X-ray spectroscopy (EDS) detectors. Image analysis for estimating the porosity of the external oxide scale was carried out with ImageJ software by averaging the area fraction of the porosity in 3 random regions which covered over 800 μm^2 area each within the external oxide scale.

Table 1

Compositions (in at%) of the studied alloy samples determined by EDS.

Alloy	Al	Cr	Mo	Nb	Ta	Ti	V	Zr
R0	-	-	-	24.9±0.6	27.1±1.4	22.8±1.2	-	25.3±1.2
R1	18.0±1.1	-	-	21.0±0.0	20.1±2.1	19.3±0.2	-	22.1±1.5
R1-Nb	19.0±0.8	-	-	-	25.6±2.3	25.7±0.5	-	29.8±1.5
R1-Ta	18.1±0.4	-	-	27.2±0.4	-	26.4±0.5	-	28.3±0.3
R1-Ti	19.3±0.9	-	-	24.0±0.8	24.9±0.2	-	-	31.8±0.1
R2	21.4±1.6	-	-	26.4±0.4	27.9±0.7	24.4±0.5	-	-
R2+Cr	19.5±0.0	19.5±0.4	-	20.2±0.1	21.4±0.4	19.5±0.3	-	-
R2+Mo	20.1±2.9	-	20.4±1.1	19.9±0.7	20.7±0.7	19.0±0.5	-	-
R2+V	18.7±0.4	-	-	20.9±0.3	22.2±0.4	19.0±0.2	19.2±0.1	-

3. Results

3.1 *Microstructures prior oxidation*

According to Figure 2(a), XRD analysis indicated that all alloys of interest in as-cast state have mainly body-centred-cubic (BCC) structure. Minor intermetallic phases, including C14 Laves and tetragonal Zr_2Al phases, are observed in R2+Cr and

R1-Ti, respectively. Additionally, diffraction peaks from B2 phase are detected in R1-Nb, R1-Ta, R2+Cr, R2+Mo, and R2+V, suggesting that chemical ordering may occur in these alloys.

SEM microstructures are shown in Figure 2(b)~(j) and EDS analysis are summarized in Table 2. It is evident that elements with high melting point, such as Ta, Mo, and Nb, tend to segregate toward dendrite arms (Region 1, 3, 6, 8, 10, 13, 15, 18, 20), while those with relatively low melting points, such as Zr, Ti, and Al, prefer to segregate toward inter-dendritic regions (Region 2, 4, 7, 9, 12, 14, 17, 19, 21). Region 11 in Table 2 shows an example of compositions in-between the dendrite arms and inter-dendritic regions of R1-Ti. Further examination showed that in addition to the tetragonal Zr_2Al (Region 12) and C14 Laves phase (Region 16) detected by XRD, (Zr, Al)-rich phase existed in the inter-dendritic regions of R1, Region 5. The low volume fraction of such phase is likely the reason why it was not detected by XRD.

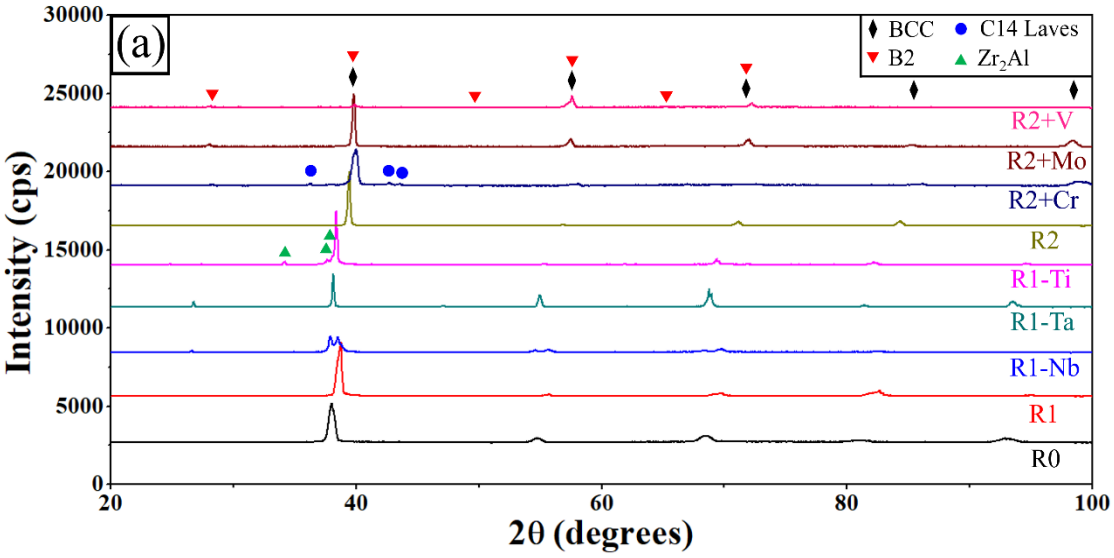

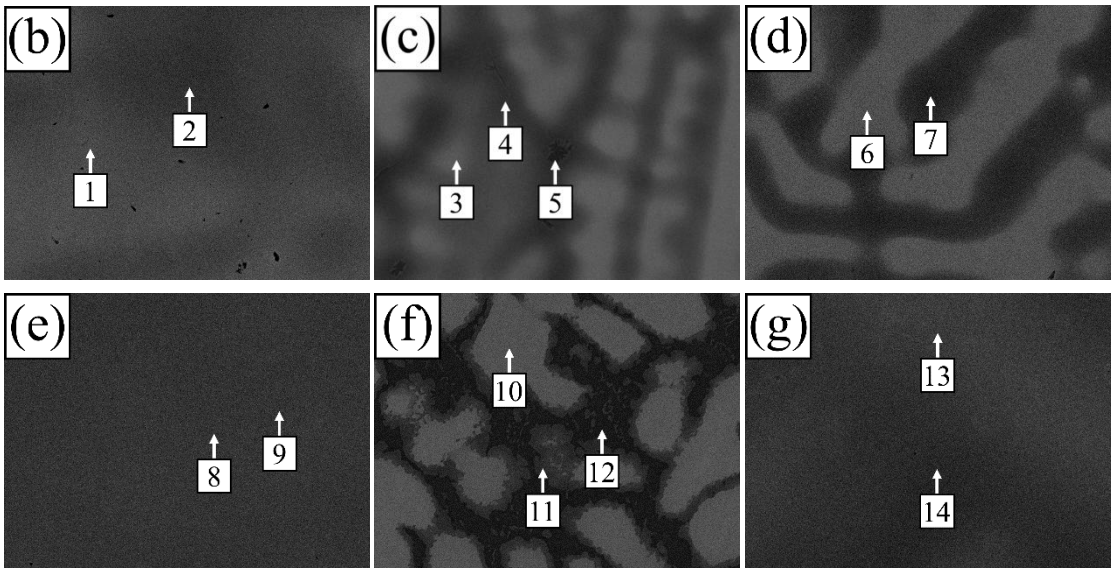

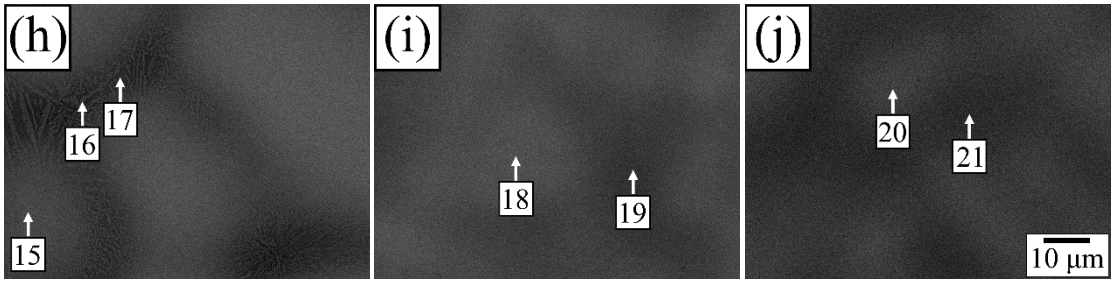

Figure 2 (a) XRD patterns of all studied RCCAs and microstructural BSE images of the as-cast (b) R0 (c) R1 (d) R1-Nb (e) R1-Ta (f) R1-Ti (g) R2 (h) R2+Cr (i) R2+Mo (j) R2+V.

Table 2

Chemical compositions (in at%) of the indicated regions in Figure 2(b)~(j).

Region	Al	Cr	Mo	Nb	Ta	Ti	V	Zr
1 (R0)	-	-	-	28.8±0.5	36.9±0.3	18.1±0.3	-	16.3±0.5
2 (R0)	-	-	-	24.0±1.3	20.6±2.6	23.4±1.0	-	32.1±3.0
3 (R1)	11.0±0.6	-	-	26.5±0.3	33.3±1.2	18.5±0.6	-	10.7±0.2
4 (R1)	26.4±0.2	-	-	12.0±1.9	6.0±2.2	19.4±1.0	-	36.3±3.8
5 (R1)	34.2±0.4	-	-	8.3±0.5	3.4±0.4	10.6±0.4	-	43.6±1.1
6 (R1-Nb)	12.2±0.6	-	-	-	44.5±0.1	26.7±0.3	-	16.7±0.2
7 (R1-Nb)	22.5±0.2	-	-	-	14.8±1.0	25.2±0.0	-	37.6±0.8
8 (R1-Ta)	16.9±0.9	-	-	30.1±0.9	-	27.0±0.8	-	26.0±0.7
9 (R1-Ta)	18.1±0.4	-	-	27.2±0.4	-	26.4±0.5	-	28.3±0.3
10 (R1-Ti)	8.1±0.3	-	-	35.3±0.3	46.4±0.3	-	-	10.3±0.5
11 (R1-Ti)	24.0±1.7	-	-	21.5±1.7	11.4±2.4	-	-	43.0±3.9
12 (R1-Ti)	35.3±0.4	-	-	13.0±0.5	5.7±0.0	-	-	46.0±0.5
13 (R2)	18.6±0.4	-	-	27.1±0.0	33.7±0.8	20.6±0.7	-	-
14 (R2)	21.7±1.1	-	-	26.4±0.3	26.6±2.1	25.5±1.1	-	-
15 (R2+Cr)	16.1±0.0	13.4±0.1	-	23.4±0.6	31.1±0.2	16.0±0.3	-	-
16 (R2+Cr)	19.4±0.3	33.8±2.1	-	15.4±0.6	15.3±0.9	16.3±1.7	-	-
17 (R2+Cr)	24.4±1.0	13.3±2.5	-	20.4±1.1	12.4±2.0	29.5±2.9	-	-
18 (R2+Mo)	11.5±1.9	-	24.8±1.0	20.6±0.2	28.8±2.1	14.3±1.2	-	-
19 (R2+Mo)	22.3±2.1	-	17.6±1.4	20.7±0.4	15.6±2.1	23.8±1.7	-	-
20 (R2+V)	17.8±0.2	-	-	21.0±0.2	25.5±0.7	17.4±0.5	18.4±0.3	-
21 (R2+V)	19.7±0.2	-	-	20.5±0.2	19.0±0.8	20.8±0.3	20.0±0.3	-

3.2 *Thermogravimetric analysis*

Figure 3 illustrates the oxidation kinetics of the studied RCCAs at 1000 ˚C for up to 2 hours. The TGA for R1-Ti and R2+V was waived owing to heavy oxidation or contamination of these alloys that could damage the instrument. The oxidation mass gain after 2 hours of isothermal oxidation at 1000 ˚C was 33.4, 19.3, 17.0, 12.2, 5.7, 1.8, and 1.0 mg/cm^2 for R0, R1-Ta, R1-Nb, R1, R2, R2+Mo, and R2+Cr, respectively. All tested RCCAs showed no noticeable spallation, except R0 had spallation from the extruding oxide formed along the corners of the specimen. But since the metallographic observation was carried out at the flat surfaces of the specimen, such spallation is not expected to affect the observation and measurement in the following sections.

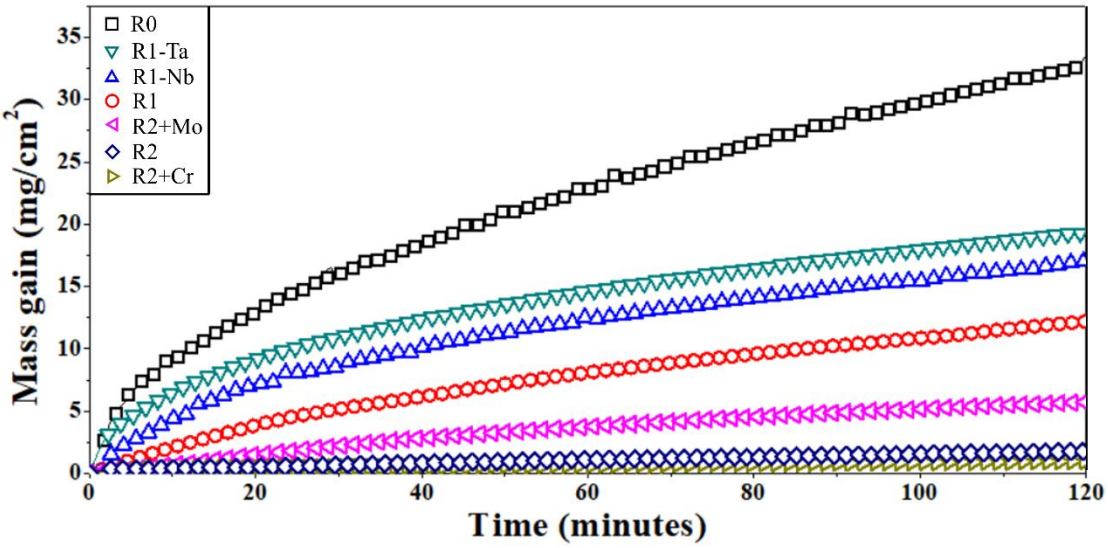

Figure 3 Oxidation mass gain curves of the studied RCCAs measured at 1000 ˚C for 120 minutes.

3.3 *Oxidation: R0 and R1 alloys (Group A)*

Comparing XRD results of both R0 and R1 after 2 and 24 hours of isothermal oxidation at 1000 ˚C, all conditions appeared to render the same oxide products, Figure 4(a). Based on the relative intensity of the diffraction peaks, the main oxide product for R0 was $TiNb_2O_7$, while that for R1 were $(Al_{0.2}Nb_{0.2}Ti_{0.6})O_2$ and $Nb_2Zr_6O_{17}$ under both oxidation condition. Ta_2O_5 was also found in both alloys, while TiO_2 and $AlNbO_4$ were identified in R0 and R1, respectively. Figure 4(b)(c) and Table 3 show both alloys were oxidised prominently in the manner of internal oxidation since the morphology and chemical profile of the metallic substrate were preserved within the oxidised region, while no obvious external oxide scale was observed. Interestingly, the scales of the oxidised regions were significantly different between these alloys: The thickness of internal oxidation region (t_{IO}) was ~358 μm for R0, which was over twice as large as ~168 μm t_{IO} of R1, Figure 4(b)(c).

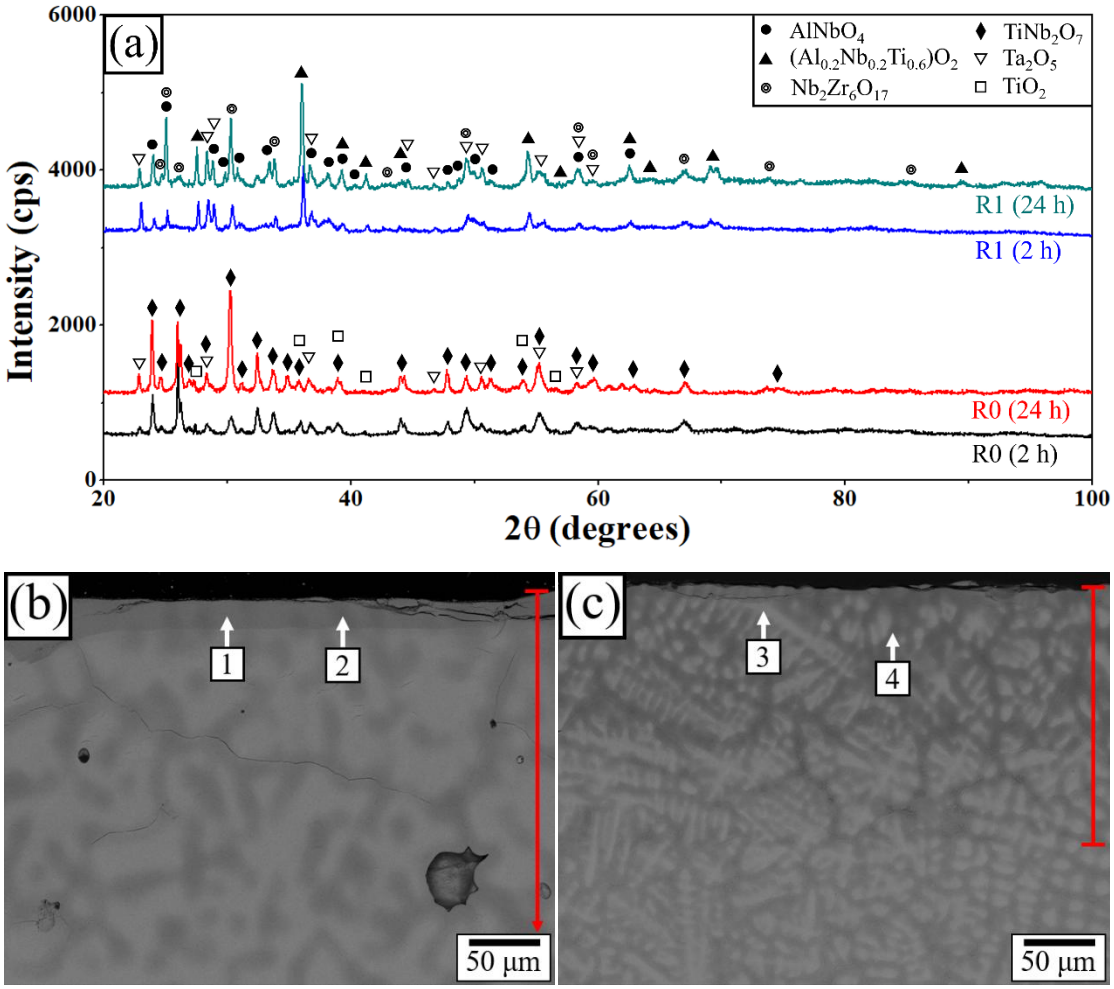

Figure 4 (a) XRD patterns of R0 and R1 after 2 and 24 hours of isothermal oxidation and cross-sectional BSE images of (b) R0 and (c) R1 after 2 hours isothermal oxidation at 1000 ˚C. The red lines in (b)(c) represent t_{IO}.

Table 3

Chemical compositions (in at%) of the indicated regions in Figure 4(b)(c). Region 1, 3 and 2, 4 are respectively the oxidised dendrite arms and inter-dendritic regions of Group A alloys.

Region	O	Al	Nb	Ta	Ti	Zr
1 (R0)	66.8±0.9	-	8.9±0.4	10.5±0.5	7.2±0.7	6.6±0.2
2 (R0)	69.1±0.5	-	7.7±0.6	6.6±0.6	7.0±0.8	9.6±0.8
3 (R1)	67.1±0.5	3.0±0.5	8.4±0.6	11.0±1.2	5.3±0.4	5.2±1.5
4 (R1)	61.8±1.5	8.4±0.8	6.0±0.7	4.7±1.0	7.5±1.0	11.6±1.5

3.4 *Oxidation: R1-Nb, R1-Ta, R1-Ti, and R2 alloys (Group B)*

Similar to that of R0 and R1, XRD analysis suggested that oxide products appeared to be the same after 2 and 24 hours of isothermal oxidation at 1000 ˚C for

R1-Nb, R1-Ta, R1-Ti, and R2, Figure 5(a). It is noteworthy that rutile-type oxides, such as $AlTaO_4$, were absent in the oxide scale of R1-Ti, which was thoroughly oxidised without any metallic part left after 24 hours of isothermal oxidation at 1000 ˚C. For R1-Nb, diffraction peaks of $AlTaO_4$ and Ta_2O_5 were prominent, while that of $Ta_2Zr_6O_{17}$ and $ZrTiO_4$ were also identified; for R1-Ta, TiO_2 and $Nb_2Zr_6O_{17}$ exhibited the highest diffraction peaks, while that of Nb_2O_5 and $AlNbO_4$ were also present. For R1-Ti, $Nb_2Zr_6O_{17}$ was the dominant oxide since its diffraction peaks were the highest among all other detected oxides. TiO_2 and Ta_2O_5 were found with high diffraction intensity for the oxide scale of R2, while $Ti_2Nb_{10}O_{29}$ was also observed.

Cross-sectional SEM-EDS analysis revealed R2 was the least oxidized, while R1-Ti was the most affected by oxidation at 1000 ˚C, Figure 5(b)~(e) and Table 4. Furthermore, Zr-containing alloys, such as R1-Nb, R1-Ta, and R1-Ti, were mainly oxidised internally while R2 showed a visible external oxidation scale and greatly reduced internal oxidation region, Figure 5(b)~(e). This could be confirmed by the strong correlation of chemical profiles between the metallic substrates and oxidised regions for R1-Nb, R1-Ta, and R1-Ti, as well as the Ti-lean external oxide scale comparing to the composition of the metallic substrate for R2, Table 2 and 4.

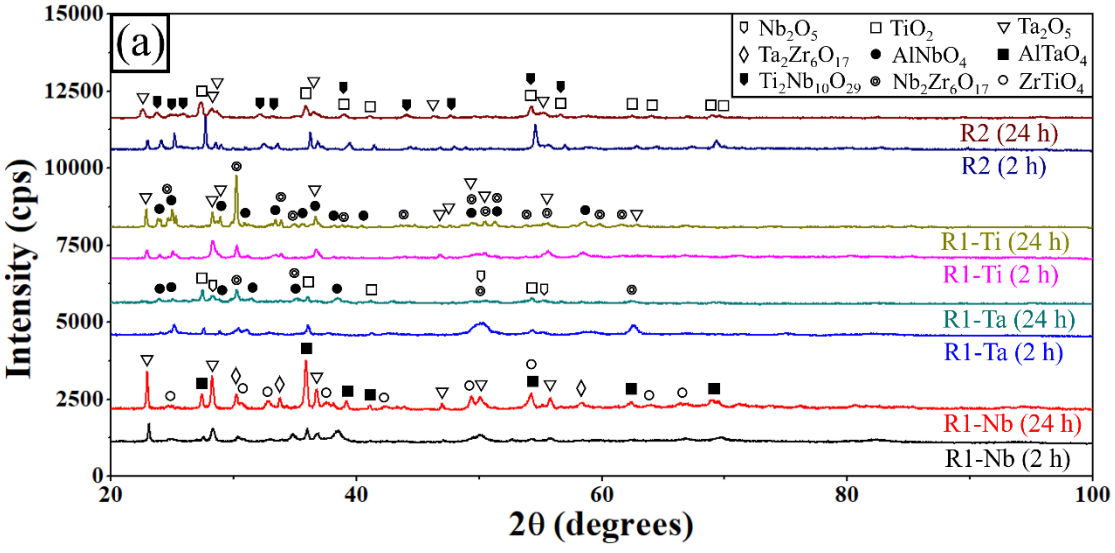

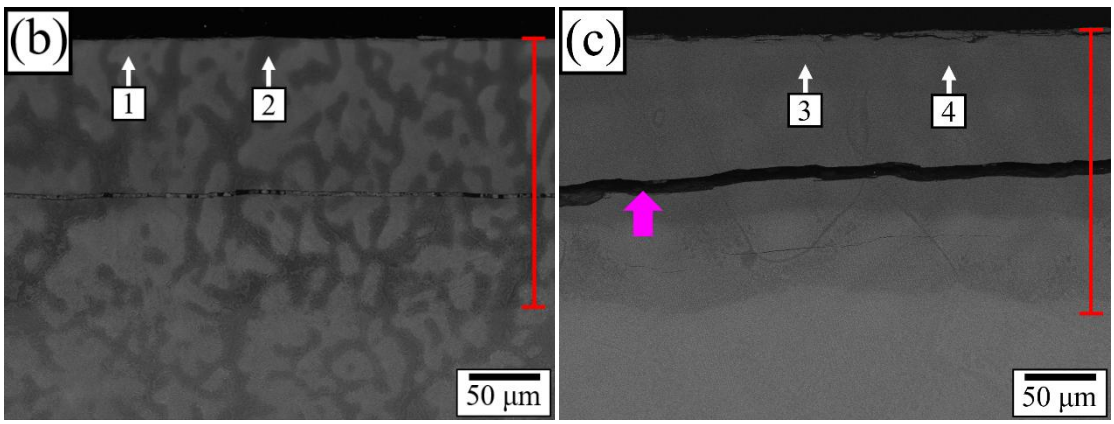

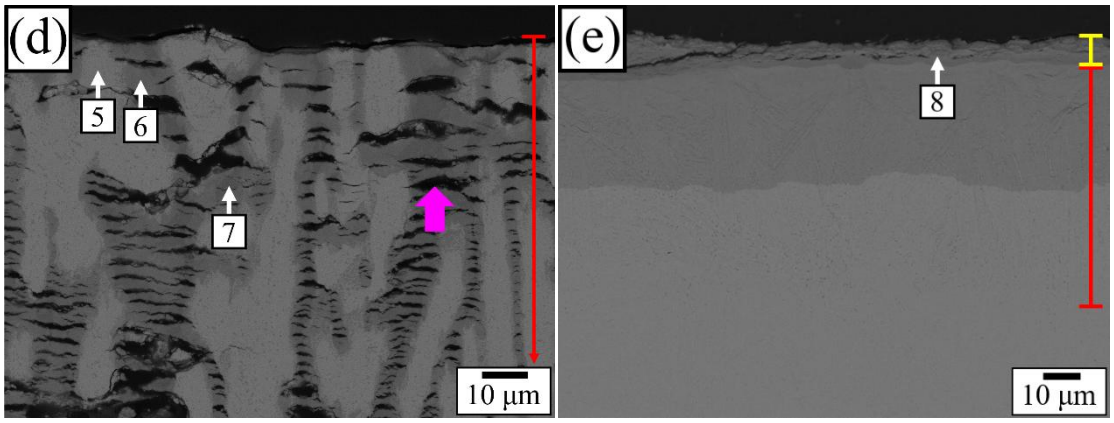

Figure 5 (a) XRD patterns of R1-Nb, R1-Ta, R1-Ti, and R2 after 2 and 24 hours of isothermal oxidation and cross-sectional BSE images of (b) R1-Nb (c) R1-Ta (d) R1-Ti (e) R2 after 2 hours of isothermal oxidation at 1000 ˚C. The yellow line in (e) marks the thickness of external oxide scale (t_{EO}) while red lines in (b)~(e) mark t_{IO}. The width of the cracks (magenta arrowheads in (c)(d)) was excluded during the thickness measurement.

Table 4

Chemical compositions (in at%) of the indicated regions in Figure 5(b)~(e). Region 1, 3, 5 and 2, 4, 7 are respectively the oxidised dendrite arms and inter-dendritic regions of R1-Nb, R1-Ta, and R1-Ti, while Region 6 and 8 are respectively the oxidised inter-diffusion zone of R1-Ti and the external oxide scale of R2.

Region	O	Al	Nb	Ta	Ti	Zr
1 (R1-Nb)	48.7±2.4	5.4±0.7	-	25.9±2.3	12.5±0.6	7.4±0.4
2 (R1-Nb)	61.2±1.6	9.2±0.9	-	5.9±1.6	9.2±1.4	14.4±0.9
3 (R1-Ta)	55.8±1.4	8.5±0.5	13.0±1.2	-	11.1±0.2	11.5±0.3
4 (R1-Ta)	57.5±2.2	8.7±0.4	9.9±2.0	-	9.2±1.6	14.8±1.7
5 (R1-Ti)	68.9±0.1	0.7±0.3	11.2±0.2	15.8±0.2	-	3.4±0.1
6 (R1-Ti)	65.0±0.4	8.5±0.5	7.0±0.3	4.5±0.4	-	15.0±0.5
7 (R1-Ti)	62.4±1.6	12.9±1.3	4.2±1.0	1.8±0.7	-	18.8±1.3
8 (R2)	68.5±0.7	6.9±1.1	9.1±0.8	10.2±0.9	5.3±0.5	-

3.5 *Oxidation: R2+Cr, R2+Mo, and R2+V alloys (Group C)*

XRD analysis indicated that R2+Mo formed $MoTaTi_8O_{25}$, $AlTiTaO_6$, and $AlNbO_4$ after both 2 and 24 hours of isothermal oxidation, while the oxides observed in R2+Cr and R2+V were slightly different under these oxidation conditions, Figure 6(a). For R2+Cr, diffraction peaks of $AlTaO_4$ were pronounced under both conditions, while that of Ta_2O_5 were only found after 2 hours of isothermal oxidation. In the case

of R2+V, only the diffraction peaks from $AlNbO_4$ were identified after 2 hours, while that of VTa_9O_{25} and $AlTaTiO_6$ were detected after 24 hours of isothermal oxidation.

Cross-sectional SEM-EDS analysis showed all alloys in this group formed external oxide scale within 2 hours at 1000 ˚C, Figure 6(b)(d)(f) and Table 5. In addition to minor Al-rich oxide (Region 1) and Ta_2O_5 (Region 2), the external oxide scale of R2+Cr contained $AlTaO_4$ (Region 3) with $CrTaO_4$ dispersion (Region 4) and it was ~14 μm in thickness, which was the thinnest t_{EO} in this group. The external oxide scale of R2+Mo was ~48 μm thick and mainly composed of $AlTiTaO_6$ (Region 5) and $MoTiTa_8O_{25}$ (Region 6), while that of R2+V was 267 μm thick and consisted of $AlNbO_4$ (Region 7), VTa_9O_{25} (Region 8), and $AlTiTaO_6$ (Region 9), Figure 6(c)(e)(g). In terms of internal oxidation, R2+Mo showed only ~4 μm of t_{IO}, which was the thinnest t_{IO} in all studied alloys.

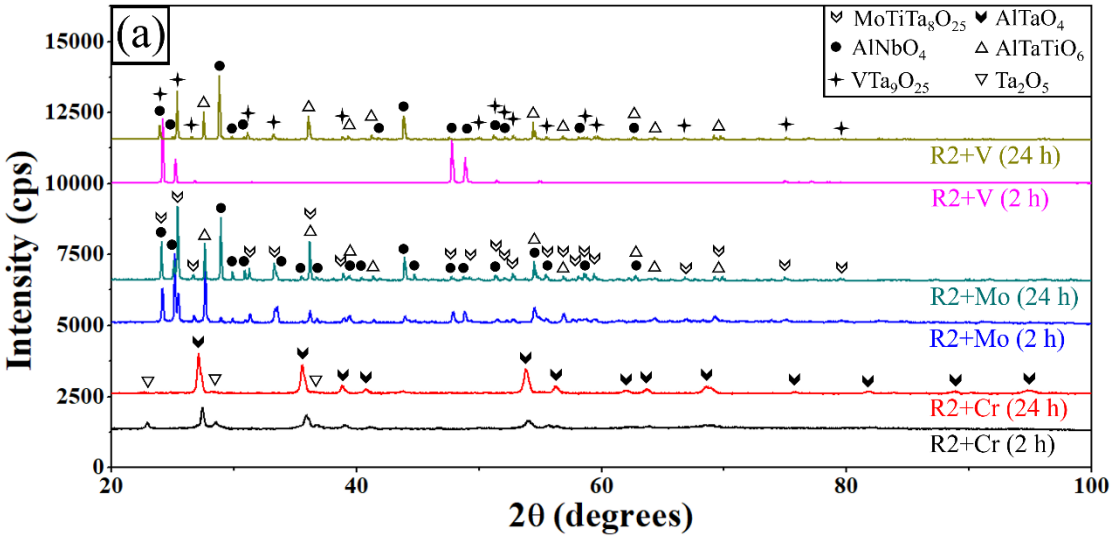

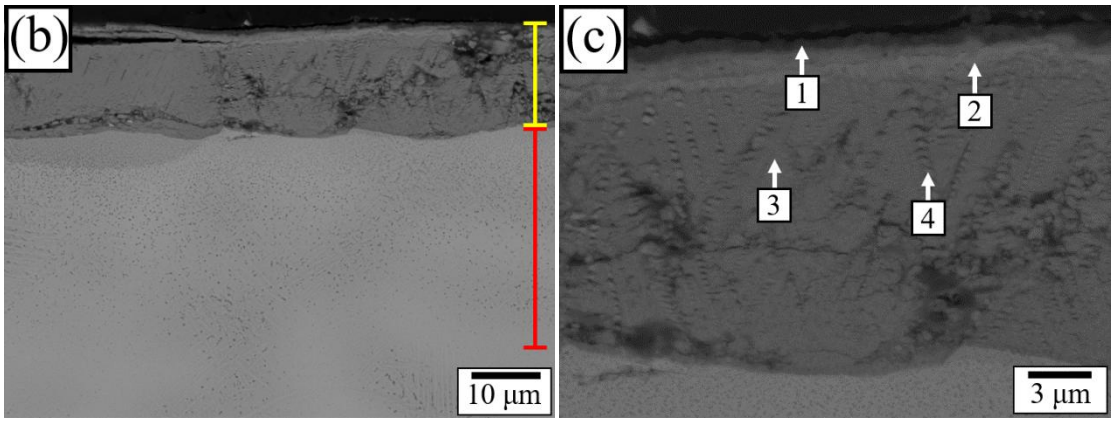

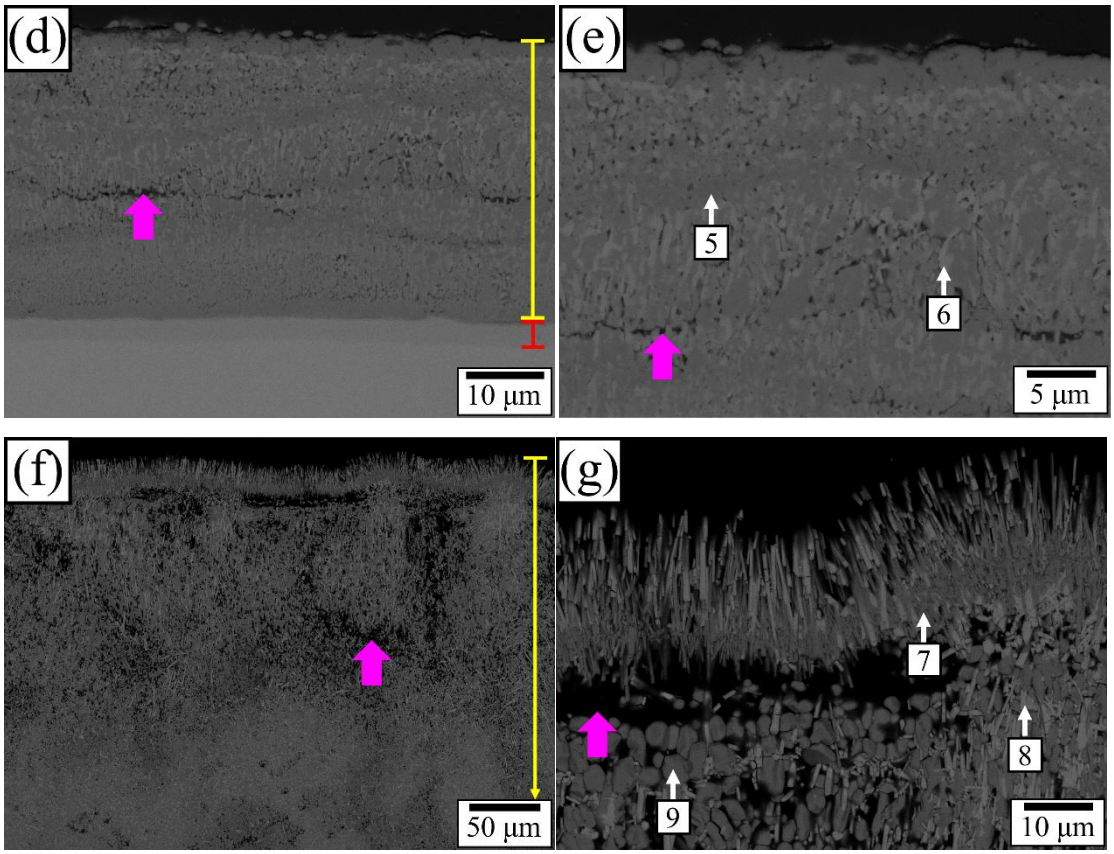

Figure 6 (a) XRD patterns of R2+Cr, R2+Mo, and R2+V after 2 and 24 hours of isothermal oxidation and cross-sectional BSE images of (b)(c) R2+Cr (d)(e) R2+Mo (f)(g) R2+V after 2 hours of isothermal oxidation at 1000 ˚C. The yellow and red lines in (b)(d)(f) respectively mark t_{EO} and t_{IO}, while the magenta arrowheads in (d)~(g) indicate the pores caused by evaporation of volatile oxides in the external oxide scale.

Table 5

Chemical compositions (in at%) of the indicated regions in Figure 6(c)(e)(g).

Region	O	Al	Cr	Mo	Nb	Ta	Ti	V
1 (R2+Cr)	69.9±1.9	13.7±1.6	6.5±0.6	-	1.5±0.2	1.0±0.2	7.3±1.7	-
2 (R2+Cr)	69.4±0.3	5.4±0.5	1.3±0.0	-	8.8±0.2	9.3±0.3	5.8±0.5	-
3 (R2+Cr)	67.1±0.9	6.9±0.7	6.2±0.5	-	6.6±0.4	7.4±0.2	5.8±0.3	-
4 (R2+Cr)	66.1±1.1	7.0±0.3	8.7±0.8	-	6.1±0.4	7.9±0.6	4.3±0.6	-
5 (R2+Mo)	65.9±0.6	12.6±0.7	-	0.5±0.2	7.5±0.9	6.3±0.4	7.1±1.3	-
6 (R2+Mo)	69.0±0.8	3.9±1.0	-	2.8±0.5	10.6±0.8	9.7±0.6	4.0±0.7	-
7 (R2+V)	58.5±5.0	14.1±1.1	-	-	10.1±1.3	6.9±1.0	6.7±1.1	3.8±0.7
8 (R2+V)	66.7±2.4	0.4±0.3	-	-	15.0±1.7	12.0±0.7	1.9±0.2	4.0±0.5
9 (R2+V)	62.1±1.6	9.8±0.4	-	-	4.8±0.3	7.4±0.2	10.8±0.9	5.2±0.8

4. Discussion

Experimental results suggest that TGA and the total thickness of oxidation-affected region (t_O = t_{EO} + t_{IO}) measurement generally show good agreement with each other, Figure 3 and 7. The addition of Al decreases, while Zr addition could increase both oxidation mass gain and t_O in this work. For Group A, t_O of R1 was 53 % thinner and oxidation mass gain was 63 % lower than that of R0 following Al addition; for Group B, t_O of R2 was 53 % thinner and oxidation mass gain was 53 % lower than that of the other Zr-bearing RCCAs following the removal of Zr. Furthermore, the results suggest that Ti might be crucial for the oxidation resistance of RCCAs since R1-Ti, which was the only Ti-free RCCA in this study, thoroughly oxidised with no metallic part left after 24 hours of isothermal oxidation at 1000 ˚C. The results of R2+Mo and R2+V further reveal that Mo addition might suppress internal oxidation but form an external oxide scale with porosity, while V addition was clearly devastating for oxidation resistance. Cr addition appeared to greatly improve oxidation resistance since R2+Cr showed the lowest oxidation mass gain and t_O among all studied alloys. The oxides observed in the present study rarely possessed simple compositions, such as Al_2O_3 and Cr_2O_3. Since current understanding on the properties of these complex oxides is still strictly limited, it is important to examine and deduce the characteristics of these oxides that could be important for future alloy design.

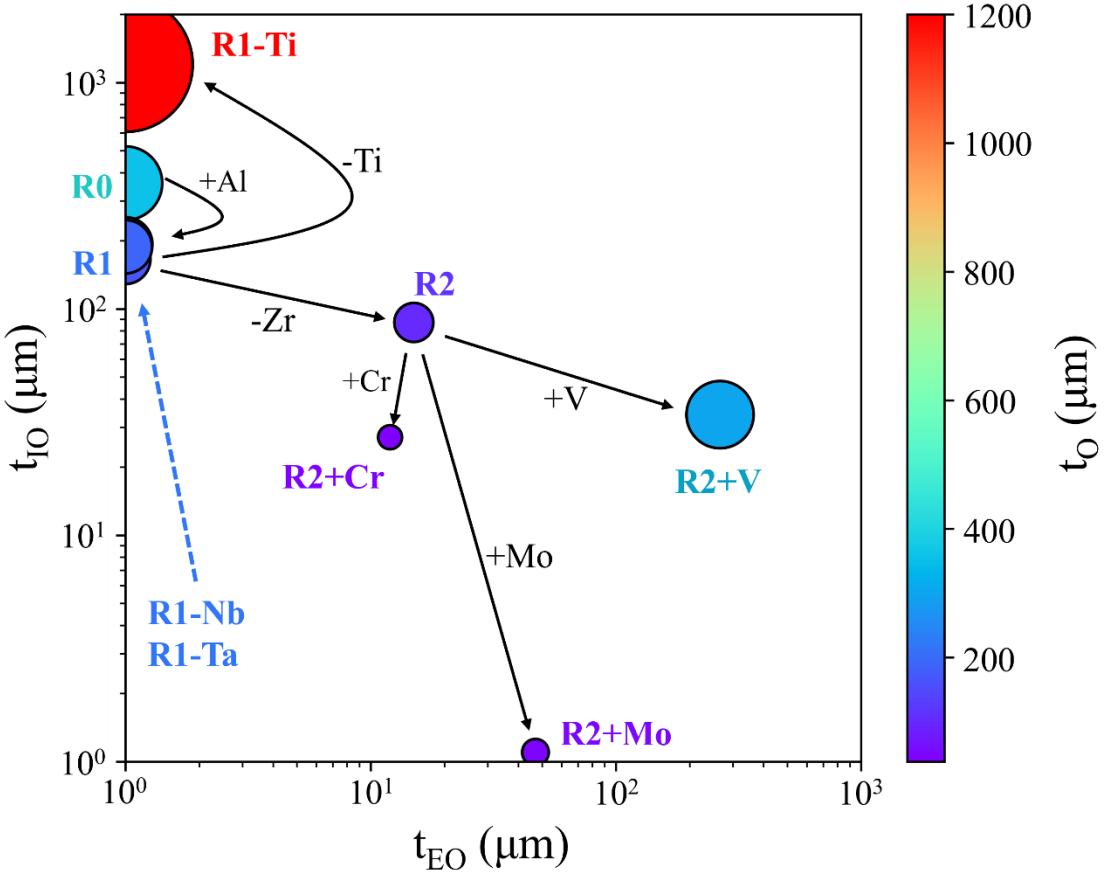

Figure 7 t_{EO}, t_{IO}, and t_O of the studied RCCAs after 2 hours of isothermal oxidation at 1000 ˚C.

4.1 *The effects of Al, Cr, Nb, Ta, and Ti addition*

Traditionally, the surface stability of an alloy can be related to the formation of a continuous and protective oxide scale [8, 33, 34], which can be achieved by alloying with protective-oxide-forming elements or modified matrix properties, such as the oxygen solubility [8, 33, 51]. For Al and Cr, both elements are frequently added to enhance oxidation resistance, since Al_2O_3 and Cr_2O_3 scales have been proven to be effective barriers [34]. However, in the present study, both protective oxide scales were not observed. Instead, rutile-type Al- and Cr- bearing complex oxides, such as $AlTaO_4$ and $CrTaO_4$ or their related oxides, were observed in most of the studied alloys.

Despite the absence of Al_2O_3 and Cr_2O_3, these complex oxides seem to provide reasonable protection against oxidation, especially in the case of R2+Cr, since it formed a continuous rutile-type complex oxide scale, Figure 6 and 7. The prominent peak intensity of rutile-type $(Al_{0.2}Nb_{0.2}Ti_{0.6})O_2$ for R1 also corresponded with its greatly reduced t_O and oxidation mass gain comparing to R0, Figure 4(a) and 7. This observation agrees with that observed in previous literatures [20, 21, 23, 24], in which the formation of rutile-type $CrTaO_4$-based oxide could improve the oxidation resistance of RCCAs. It is also proposed that while Cr addition could promote formation of rutile-type oxides such as $CrNbO_4$ and $CrTaO_4$, the formation of $CrTaO_4$ would be more favourable than that of $CrNbO_4$ owing to its more negative formation free energy [21]. But since other factors, such as the kinetics of oxide growth and oxygen permeability of the oxide, are also essential for the formation of a protective oxide layer, whether $CrTaO_4$ is preferable to $CrNbO_4$ as the protective oxide layer requires further study to be clarified.

Interestingly, while the oxidation of R1-Nb and R1-Ta showed no noticeable difference in terms of t_{EO}, t_{IO}, and t_O, the mass gain of R1-Nb was 2.3 mg/cm^2 lower than that of R1-Ta after isothermally oxidised at 1000 ˚C for 2 hours, Figure 3 and 7. It appears that the Ta-rich dendrite arms in R1-Nb had reduced oxygen intake, while its interdendritic regions had similar oxygen intake comparing to that of the dendrite arms and interdendritic regions of R1-Ta, Table 4. Given both RCCAs had similar t_O, R1-Nb would ingest less oxygen and thus have lower oxidation mass gain than R1-Ta. While Ta and Nb are usually considered similar in terms of their chemical properties owing to their adjacent locations in the Periodic Table, Ta was found to have more pronounced effect on reducing the oxidation mass gain of TiAl-based intermetallics at 1000 ˚C comparing to Nb by decreasing the diffusion rate of oxygen [52]. These

observations suggest that the addition of Ta could be slightly superior to Nb in terms of oxidation resistance.

Furthermore, it appears that the formation of rutile-type oxides, including TiO_2, $AlTaO_4$, $CrTaO_4$ and their related oxides is generally beneficial for oxidation resistance since R1-Ti did not form rutile-type oxide and was severely oxidised within 2 hours at 1000 ˚C. While the positive effects of rutile-type oxides have been reported previously [20, 21, 23, 24, 53-56], the origin for the formation of the rutile-type oxides remains an intriguing subject for further investigation. TiO_2 is one of the most common oxides that possesses rutile-type crystal structure; when more than 2 refractory elements are co-oxidised, Ti can also be solutioned in rutile-type complex oxides [20, 24]. While Al and Ta can form rutile-type $AlTaO_4$ when their oxides react with each other [57], rutile-type oxide was not detected in the oxide scale of R1-Ti. Therefore, the presence of Ti could benefit the oxidation resistance of RCCAs by promoting the formation of rutile-type oxide.

4.2 *The effects of Mo addition*

Since MoO_3 would sublimate at 800 ˚C and above [58], the oxidation of Mo is definitely not the reason behind the reduced t_O of R2+Mo. Since R2+Mo showed the thinnest t_{IO} among all tested RCCAs in the present study, it could be postulated that the internal oxidation was suppressed due to the presence of Mo. Considering a binary alloy system M-Al, in which M is an oxygen-soluble arbitrary metal nobler than Al and Al is a dilute solute. Here, if Al_2O_3 is thermodynamically very stable and the diffusivity of Al is significantly lower than that of oxygen, the time (t) dependency for the depth of internal oxidation (ξ) of such alloy can be described as [8]:

$$\xi(t) \propto \sqrt{N_O^{(s)} t} \ldots\ldots\ldots (1)$$

In which $N_O^{(s)}$ is the oxygen solubility of the alloy substrate. Such relationship indicates that reduced $N_O^{(s)}$ would suppress internal oxidation. Generally, the internal oxidation is not desirable for the oxidation resistance of an alloy since the protective oxide scale is formed via external oxidation. Upon the formation of a continuous external oxide scale, it could act as a barrier and retard the oxidation of the alloy. Although the capabilities of such barrier depend on several factors, such as its integrity, gas permeability, and gas diffusivity, the formation of an external oxide scale and reduced internal oxidation are beneficial for the oxidation resistance of the alloy. Previous study suggested Mo possesses extremely low oxygen and nitrogen solubility as pure element [16] and it could improve the surface stability of TiAl-based alloys by decreasing the solubility of oxygen and nitrogen in the alloy substrate [59, 60]. Consequently, the reduced internal oxidation of R2+Mo might

result from the decreased $N_O^{(s)}$ caused by Mo addition. On the other hand, the external oxide scale of R2+Mo was relatively thick and full of rounded pores comparing to that of R2+Cr, indicating the former oxidised more severely than the later and might suffer from the formation and evaporation of volatile oxides, Figure 6. The area fraction of the rounded pores was estimated to be 2.4 % according to the image analysis. Since R2+Mo contains 20 at% of Mo, it is possible that volatile oxides, such as MoO_3, would form during the isothermal oxidation at 1000 ˚C. Furthermore, the tetragonal $MoTiTa_8O_{25}$ was present in the oxide scale of R2+Mo alloy. Despite its presence was mentioned in the oxidation of $CrMo_{0.5}NbTa_{0.5}TiZr$ [47], no further description regarding to its properties was discussed. In this work, the formation of $MoTiTa_8O_{25}$ could result from a reaction among MoO_3, TiO_2, and Ta_2O_5 in Ta_2O_5-rich environment:

$$MoO_3 + TiO_2 + 4Ta_2O_5 = MoTiTa_8O_{25} \text{…….. (2)}$$

Since $MoTiTa_8O_{25}$ is largely preserved while MoO_3 is not found in the oxide scale of R2+Mo after the isothermal oxidation at 1000 ˚C, the thermal stability of $MoTiTa_8O_{25}$ should be superior to that of MoO_3. It appears that $MoTiTa_8O_{25}$ prevented heavy evaporation of MoO_3 by forming an external oxide scale since there was no obvious MoO_3 residue in the crucible after the oxidation test. Therefore, the oxidation mass loss caused by MoO_3 in the present study could be neglectable at least up to 2 hours of isothermal oxidation at 1000 ˚C. But considering the relatively thick oxide scale of R2+Mo comparing with that of R2+Cr, such oxide is not likely to be an efficient oxygen barrier. These could be the reasons why R2+Mo has thicker and more porous external oxide scale comparing to that of R2+Cr.

4.3 *The effects of Zr and V addition*

According to the oxidation behaviours of Zr- and V-bearing RCCAs, it appears that both alloying additions were detrimental since they are associated with large oxidation mass gain or t_O for RCCAs, Figure 1 and 7. While Zr is a common constituent in ductile RCCAs [41, 42, 44, 45, 61], ZrO_2, which is a common form of Zr-related oxide, is known for its detrimental effects due to its polymorphism properties across a wide range of temperature [62, 63]. However, since ZrO_2 was not detected in this work, its role on oxidation might not be so direct. Alternatively, ZrO_2 could react with other refractory oxides, such as TiO_2 and Nb_2O_5, to form complex refractory oxides, such as $ZrTiO_4$ [63-66] and $Nb_2Zr_6O_{17}$ [37]. Interestingly, $Ta_2Zr_6O_{17}$ was additionally found in the present study, presumably it was formed due to a reaction between ZrO_2 and Ta_2O_5. Despite there has been no literature specifically describing the properties of these Zr-related complex refractory oxides, it is not likely that these oxides are protective against oxidation since these Zr-bearing alloys show

poor oxidation resistance [37, 63]. RCCAs containing Zr as main constituent could suffer from heavy internal oxidation owing to the high affinity and solubility with oxygen and nitrogen of Zr [67], which agrees with the observation in the present study, Figure 3 and 7. On the other hand, although V has high solubility for oxygen [67, 68], V_2O_5 could melt and become volatile at above 690 ˚C [69]. In this work, the Al_2O_3 crucible used as the container for R2+V was heavily contaminated after the 24 hours of isothermal oxidation at 1000 ˚C. Along with large pores shown in Figure 6, which were 8.2 % in area fraction within the oxide scale of R2+V, it is reasonable to assume that the formation and melting of V_2O_5 occurred during the test. Another noticeable V-related oxide found in R2+V was the tetragonal VTa_9O_{25}, which has not been reported in the literature regarding to the oxidation of RCCAs. While its impact on the surface stability of RCCAs is unknown, it has been suggested that VTa_9O_{25} is a stable oxide at the Ta_2O_5-rich end of V_2O_5-Ta_2O_5 quasi-binary phase diagram and it could melt at around 1800 ˚C [70]. Therefore, it is likely that some of the V_2O_5 reacted with Ta_2O_5 and formed VTa_9O_{25} instead of melting away during the oxidation of R2+V at 1000 ˚C via the following reaction:

$$1/2\ V_2O_5 + 9/2\ Ta_2O_5 = VTa_9O_{25} \quad \ldots\ldots\ldots (3)$$

Since VTa_9O_{25} possesses much higher melting point than that of V_2O_5, the formation of VTa_9O_{25} might be less harmful to the surface stability of RCCAs than that of V_2O_5.

4.4 *The characteristics of complex oxides*

The other group of complex oxides identified in this work includes $AlNbO_4$, $TiNb_2O_7$, and $Ti_2Nb_{10}O_{29}$. In previous studies, these oxides were found when Nb content was high enough to reach its solubility limits in TiO_2 for TiAl-based alloys [71, 72] or when Nb_2O_5 could react with Al_2O_3 in Nb-based alloys [56, 73]. Interestingly, the effects of these oxide on the surface stability of the reported alloys can be either positive or negative. For TiAl-based alloys, the formation of $TiNb_2O_7$ could deteriorate oxidation resistance by interrupting the Nb-doped TiO_2 scale, which could have assisted the formation of a continuous Al_2O_3 scale [71, 72]; on the other hand, the formation of $AlNbO_4$ could enhance oxidation resistance of Nb-based alloys by increasing the integrity of the oxide scale [56]. While the role of $Ti_2Nb_{10}O_{29}$ on the surface stability has not been specifically described in the literature, it is frequently found in the oxide scale of Ti-bearing and Nb-based alloys and could decompose into $TiNb_2O_7$ [74, 75]. It is evident that these oxides would not be effective oxygen barriers comparing to Al_2O_3, Nb-doped TiO_2, or rutile-type oxide like $CrNbO_4$ [71, 72, 76]. Therefore, the formation of these oxides should be avoided when designing RCCAs that form protective oxide scale at high temperature, and this could be

achieved by limiting Nb content in RCCAs.

Multiple complex refractory oxides have been observed instead of simple oxides, such as Al_2O_3 and ZrO_2, in the present study. Here, the simple oxides might react with each other and form complex oxides rather than existing independently, or the complex oxides were directly formed as the stable oxides in the studied system. In both cases, the formation free energy of the complex oxides could be more negative than that of the simple oxides. However, such data cannot be retrieved from current thermodynamic databases despite they do contain the constituents of the present alloys. This is because these databases have been developed for a particular alloy family, so each database can only accurately describe the corner region of the phase diagram containing the main element. Although thermodynamic databases dedicated to high entropy alloys has been intensively developed, they currently contain a very limited number of assessed ternaries with oxygen. Still, the TCOX11 database for Thermo-Calc Software dedicated to the thermodynamic simulation of oxides allows the clarification to the formation of the intermediate oxide $ZrTiO_4$ in Ti-O-Zr bearing alloys. As shown in Figure 8, three ternary oxides adjacent to both phase fields with ZrO_2 and TiO_2 exist with different stability range. Above 1150 ˚C, the disordered □-$Zr_xTi_{1-x}O_4$ crystallizes in an orthorhombic structure. At lower temperatures, it undergoes two ordering transitions to α-$ZrTiO_4$, and α'-$ZrTiO_4$ below 1050 ˚C. This could help explaining the presence of $ZrTiO_4$ in the oxide layer of some (Zr, Ti)-bearing alloys [63, 65, 66], including R1-Nb in this study.

In summary, the content of Al, Cr, and Ti in RCCAs could benefit the oxidation resistance by forming rutile-type complex oxides, while Zr and V contents could deteriorate surface stability by forming non-protective oxides and enhancing internal oxidation; Mo addition could greatly suppress internal oxidation of the substrate, but the formation of non-protective $MoTiTa_8O_{25}$ might lead to reduced resistance against oxidation; Ta addition could be slightly more beneficial than Nb addition in terms of oxidation resistance owing to reduced oxygen intake of the alloy bulk. The properties and the parent alloys of the observed oxides in the present study are summarized in Table 6. The formation of oxides and their growth kinetics are heavily composition dependent, thus changing the alloying amount of each element could lead to different oxidation kinetics. These results and discussions present in this article could provide guidelines for the design of RCCA with improved oxidation resistance in the future.

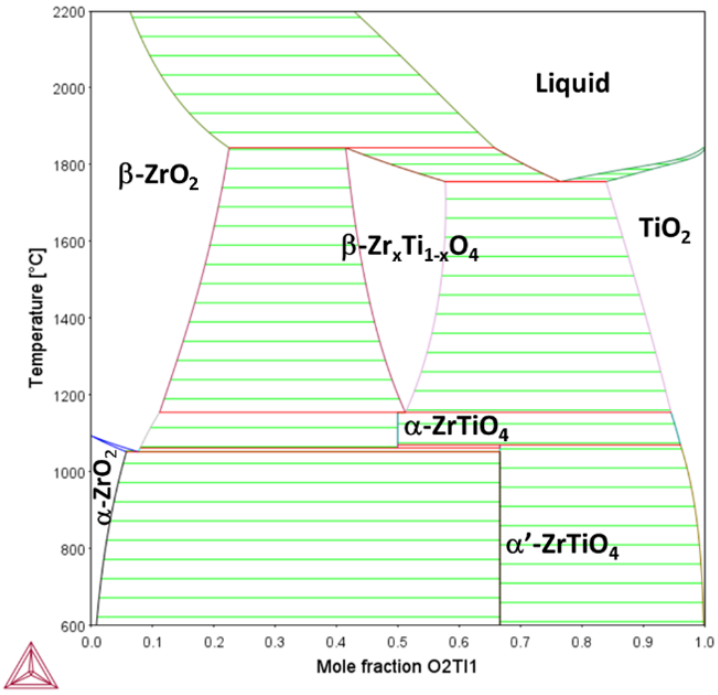

Figure 8 ZrO_2-TiO_2 ternary phase diagram calculated with Thermo-Calc Software equipped with TCOX11 database.

Table 6

The constituents, crystal structures, and the parent alloys of the observed oxides in this work.

Element	Combination	Oxide	Crystal Structure	Alloy(s)
Al	Nb	$AlNbO_4$	Monoclinic	R1 R1-Ta R1-Ti R2+Mo R2+V
	Ta	$AlTaO_4$	Tetragonal (rutile)	R2+Cr
	Nb, Ti	$(Al_{0.2}Nb_{0.2}Ti_{0.6})O_2$	Tetragonal (rutile)	R1
	Ta, Ti	$AlTaTiO_6$	Tetragonal (rutile)	R1-Nb R2+Mo R2+V
Cr	Ta	$CrTaO_4$	Tetragonal (rutile)	R2+Cr
Mo	Ta, Ti	$MoTiTa_8O_{25}$	Tetragonal	R2+Mo
V	Ta	VTa_9O_{25}	Tetragonal	R2+V
Zr	Nb	$Nb_2Zr_6O_{17}$	Orthorhombic	R1 R1-Ta R1-Ti

	Ta	$Ta_2Zr_6O_{17}$	Orthorhombic	R1-Nb
	Ti	$ZrTiO_4$	Orthorhombic	R1-Nb
Nb	Ti	$TiNb_2O_7$	Monoclinic	R0
		$Ti_2Nb_{10}O_{29}$		R2
	-	Nb_2O_5	Monoclinic	R1-Ta
Ta	-	Ta_2O_5	Orthorhombic	R0 R1 R1-Nb R1-Ti R2 R2+Cr
Ti	-	TiO_2	Tetragonal (rutile)	R0 R1-Ta R2

5. Conclusions

Several RCCAs have been designed by systematic change in composition with respect to Al, Cr, Mo, Nb, Ta, Ti, V, Zr and subjected to isothermal oxidation for up to 24 hours at 1000 ˚C in order to examine the effects of the individual elements on oxidation. It is found that the addition of Al, Cr, and Ti could benefit the oxidation resistance by forming rutile-type complex oxides instead of their individual oxides, while the addition of Zr and V degraded the oxidation resistance by forming non-protective oxides or promoting internal oxidation. Mo addition appeared to suppress the internal oxidation, yet the formation of non-protective $MoTiTa_8O_{25}$ might undermine the surface stability. Ta addition showed slightly reduced oxidation mass gain comparing with Nb addition owing to the reduced oxygen intake of the alloy bulk in the present study. This work has presented the effects of multiple elements on the oxidation of RCCAs and their associated oxides formation, and it may provide guidelines to design future RCCAs with enhanced oxidation resistance.

Declaration of Competing Interest

The authors declare that they have no known competing financial interests or personal relationships that could have appeared to influence the work reported in this paper.

Acknowledgements

This work was financially supported by the “High Entropy Materials Centre” from The Featured Areas Research Centre Program within the framework of the

Higher Education Sprout Project by the Ministry of Education (MOE) and from the Project MOST107-2923-E-007-010-MY3, MOST109-2221-E-007-057, MOST110-2634-F-007-024, MOST110-2224-E-007-001, MOST110-2221-E-007-020-MY3 by Ministry of Science and Technology (MOST) in Taiwan. UG gratefully acknowledge the support by the Deutsche Forschungsgemeinschaft through the Priority Programme SPP 2006 "Compositionally Complex Alloys - High Entropy Alloys (CCA - HEA)". SG gratefully acknowledge the support by the CNRS through the 80 PRIME programme.

References

[1] O.N. Senkov, G.B. Wilks, D.B. Miracle, C.P. Chuang, P.K. Liaw, Refractory high-entropy alloys, Intermetallics 18 (2010) 1758-1765. http://dx.doi.org/10.1016/j.intermet.2010.05.014.

[2] O.N. Senkov, G.B. Wilks, J.M. Scott, D.B. Miracle, Mechanical properties of Nb25Mo25Ta25W25 and V20Nb20Mo20Ta20W20 refractory high entropy alloys, Intermetallics 19 (2011) 698-706. http://dx.doi.org/10.1016/j.intermet.2011.01.004.

[3] O.N. Senkov, C.F. Woodward, Microstructure and properties of a refractory NbCrMo0.5Ta0.5TiZr alloy, Materials Science and Engineering: A 529 (2011) 311-320. http://dx.doi.org/10.1016/j.msea.2011.09.033.

[4] O.N. Senkov, S.V. Senkova, C. Woodward, Effect of aluminum on the microstructure and properties of two refractory high-entropy alloys, Acta Materialia 68 (2014) 214-228. http://dx.doi.org/10.1016/j.actamat.2014.01.029.

[5] O.N. Senkov, C. Woodward, D.B. Miracle, Microstructure and Properties of Aluminum-Containing Refractory High-Entropy Alloys, JOM 66 (2014) 2030-2042. http://dx.doi.org/10.1007/s11837-014-1066-0.

[6] H. Chen, A. Kauffmann, B. Gorr, D. Schliephake, C. Seemüller, J.N. Wagner, H.J. Christ, M. Heilmaier, Microstructure and mechanical properties at elevated temperatures of a new Al-containing refractory high-entropy alloy Nb-Mo-Cr-Ti-Al, Journal of Alloys and Compounds 661 (2016) 206-215. http://dx.doi.org/10.1016/j.jallcom.2015.11.050.

[7] N.O. Senkov, D. Isheim, N.D. Seidman, L.A. Pilchak, Development of a Refractory High Entropy Superalloy, Entropy 18 (2016), e18030102. https://doi.org/10.3390/e18030102.

[8] J. Smialek, G.M. Meier, High-temperature oxidation, in: C.T. Sims, N.S. Stoloff, W.C. Hagel (Eds.) Superalloys II, Wiley-Interscience, John Wiley and Sons, United States of America, 1987, pp. 293-326.

[9] L. Huang, X. Sun, H. Guan, Z. Hu, Oxidation behavior of a single-crystal Ni-base superalloy in air at 900, 1000 and 1100° C, Oxidation of Metals 65 (2006) 207-222.

https://doi.org/10.1007/s11085-006-9016-z.
[10] M. Bensch, A. Sato, N. Warnken, E. Affeldt, R.C. Reed, U. Glatzel, Modelling of High Temperature Oxidation of Alumina-Forming Single-Crystal Nickel-Base Superalloys, Acta Materialia 60 (2012) 5468-5480. https://doi.org/10.1016/j.actamat.2012.06.036.
[11] K. Kawagishi, A.-C. Yeh, T. Yokokawa, T. Kobayashi, Y. Koizumi, H. Harada, Development of an oxidation-resistant high-strength sixth-generation single-crystal superalloy TMS-238, Superalloys 12 (2012) 189-196.
[12] B.A. Pint, K.L. More, I.G. Wright, The use of two reactive elements to optimize oxidation performance of alumina-forming alloys, Materials at High Temperatures 20 (2003) 375-386. https://doi.org/10.1179/mht.2003.044.
[13] C.M. Liu, H.M. Wang, S.Q. Zhang, H.B. Tang, A.L. Zhang, Microstructure and oxidation behavior of new refractory high entropy alloys, Journal of Alloys and Compounds 583 (2014) 162-169. http://dx.doi.org/10.1016/j.jallcom.2013.08.102.
[14] B. Gorr, M. Azim, H.-J. Christ, T. Mueller, D. Schliephake, M. Heilmaier, Phase equilibria, microstructure, and high temperature oxidation resistance of novel refractory high-entropy alloys, Journal of Alloys and Compounds 624 (2015) 270-278. https://doi.org/10.1016/j.jallcom.2014.11.012.
[15] B. Gorr, F. Mueller, H.-J. Christ, T. Mueller, H. Chen, A. Kauffmann, M. Heilmaier, High temperature oxidation behavior of an equimolar refractory metal-based alloy 20Nb 20Mo 20Cr 20Ti 20Al with and without Si addition, Journal of Alloys and Compounds 688 (2016) 468-477. https://doi.org/10.1016/j.jallcom.2016.07.219.
[16] B. Gorr, F. Müller, M. Azim, H.-J. Christ, T. Müller, H. Chen, A. Kauffmann, M. Heilmaier, High-Temperature Oxidation Behavior of Refractory High-Entropy Alloys: Effect of Alloy Composition, Oxidation of Metals 88 (2017) 1-11. https://doi.org/10.1007/s11085-016-9696-y.
[17] C.H. Chang, M.S. Titus, J.W. Yeh, Oxidation Behavior between 700 and 1300° C of Refractory TiZrNbHfTa High- Entropy Alloys Containing Aluminum, Advanced Engineering Materials 20 (2018), 1700948. https://doi.org/10.1002/adem.201700948.
[18] F. Müller, B. Gorr, H.-J. Christ, H. Chen, A. Kauffmann, M. Heilmaier, Effect of microalloying with silicon on high temperature oxidation resistance of novel refractory high-entropy alloy Ta-Mo-Cr-Ti-Al, Materials at High Temperatures 35 (2018) 168-176. https://doi.org/10.1080/09603409.2017.1389115.
[19] Y.-k. Cao, Y. Liu, B. Liu, W.-d. Zhang, J.-w. Wang, M. Du, Effects of Al and Mo on high temperature oxidation behavior of refractory high entropy alloys, Transactions of Nonferrous Metals Society of China 29 (2019) 1476-1483. https://doi.org/10.1016/S1003-6326(19)65054-5.

[20] K.-C. Lo, Y.-J. Chang, H. Murakami, J.-W. Yeh, A.-C. Yeh, An oxidation resistant refractory high entropy alloy protected by CrTaO 4-based oxide, Scientific reports 9 (2019), 7266. https://doi.org/10.1038/s41598-019-43819-x.
[21] F. Müller, B. Gorr, H.-J. Christ, J. Müller, B. Butz, H. Chen, A. Kauffmann, M. Heilmaier, On the oxidation mechanism of refractory high entropy alloys, Corrosion Science 159 (2019), 108161. https://doi.org/10.1016/j.corsci.2019.108161.
[22] P. Zhang, Y. Li, Z. Chen, J. Zhang, B. Shen, Oxidation response of a vacuum arc melted NbZrTiCrAl refractory high entropy alloy at 800–1200 °C, Vacuum 162 (2019) 20-27. https://doi.org/10.1016/j.vacuum.2019.01.026.
[23] B. Gorr, F. Müller, S. Schellert, H.-J. Christ, H. Chen, A. Kauffmann, M. Heilmaier, A new strategy to intrinsically protect refractory metal based alloys at ultra high temperatures, Corrosion Science 166 (2020), 108475. https://doi.org/10.1016/j.corsci.2020.108475.
[24] K.-C. Lo, H. Murakami, J.-W. Yeh, A.-C. Yeh, Oxidation behaviour of a novel refractory high entropy alloy at elevated temperatures, Intermetallics 119 (2020), 106711. https://doi.org/10.1016/j.intermet.2020.106711.
[25] O.A. Waseem, H.J. Ryu, Combinatorial synthesis and analysis of AlxTayVz-Cr20Mo20Nb20Ti20Zr10 and Al10CrMoxNbTiZr10 refractory high-entropy alloys: Oxidation behavior, Journal of Alloys and Compounds 828 (2020), 154427. https://doi.org/10.1016/j.jallcom.2020.154427.
[26] T.M. Butler, K.J. Chaput, Native oxidation resistance of Al20Nb30Ta10Ti30Zr10 refractory complex concentrated alloy (RCCA), Journal of Alloys and Compounds 787 (2019) 606-617. https://doi.org/10.1016/j.jallcom.2019.02.128.
[27] N. Yurchenko, E. Panina, S. Zherebtsov, G. Salishchev, N. Stepanov, Oxidation Behavior of Refractory AlNbTiVZr0.25 High-Entropy Alloy, Materials 11 (2018), 2526. https://doi.org/10.3390/ma11122526.
[28] S. Sheikh, L. Gan, A. Ikeda, H. Murakami, S. Guo, Alloying effect on the oxidation behavior of a ductile Al0.5Cr0.25Nb0.5Ta0.5Ti1.5 refractory high-entropy alloy, Materials Today Advances 7 (2020), 100104. https://doi.org/10.1016/j.mtadv.2020.100104.
[29] J. Litz, A. Rahmel, M. Schorr, Selective carbide oxidation and internal nitridation of the Ni-base superalloys IN 738 LC and IN 939 in air, Oxidation of Metals 30 (1988) 95-105. https://doi.org/10.1007/BF00656646.
[30] C.H. Konrad, L. Fuhrmann, R. Völkl, U. Glatzel, Internal oxidation with significant contribution of oxygen diffusion through the oxide phase, Corrosion Science 63 (2012) 187-192. https://doi.org/10.1016/j.corsci.2012.06.003.
[31] C.H. Konrad, R. Völkl, U. Glatzel, Determination of Oxygen Diffusion Along Nickel/Zirconia Phase Boundaries by Internal Oxidation, Oxidation of Metals 77

(2012) 149-165. https://doi.org/10.1007/s11085-011-9278-y.
[32] U. Krupp, H.-J. Christ, Selective oxidation and internal nitridation during high-temperature exposure of single-crystalline nickel-base superalloys, Metallurgical and Materials Transactions A 31 (2000) 47-56. https://doi.org/10.1007/s11661-000-0051-0.
[33] M.P. Brady, I.G. Wright, B. Gleeson, Alloy design strategies for promoting protective oxide-scale formation, JOM 52 (2000) 16-21. https://doi.org/10.1007/s11837-000-0109-x.
[34] B.A. Pint, J.R. DiStefano, I.G. Wright, Oxidation resistance: One barrier to moving beyond Ni-base superalloys, Materials Science and Engineering: A 415 (2006) 255-263. https://doi.org/10.1016/j.msea.2005.09.091.
[35] X. Wang, Y. Zhou, High-temperature oxidation behavior of Ti 2 AlC in air, Oxidation of Metals 59 (2003) 303-320. https://doi.org/10.1023/A:1023092027697.
[36] Y. Hua, Z. Rong, Y. Ye, K. Chen, R. Chen, Q. Xue, H. Liu, Laser shock processing effects on isothermal oxidation resistance of GH586 superalloy, Applied Surface Science 330 (2015) 439-444. https://doi.org/10.1016/j.apsusc.2015.01.033.
[37] T.M. Butler, K.J. Chaput, J.R. Dietrich, O.N. Senkov, High temperature oxidation behaviors of equimolar NbTiZrV and NbTiZrCr refractory complex concentrated alloys (RCCAs), Journal of Alloys and Compounds 729 (2017) 1004-1019. https://doi.org/10.1016/j.jallcom.2017.09.164.
[38] O.A. Waseem, U. Auyeskhan, H.M. Lee, H.J. Ryu, A combinatorial approach for the synthesis and analysis of AlxCryMozNbTiZr high-entropy alloys: Oxidation behavior, Journal of Materials Research 33 (2018) 3226-3234. https://doi.org/10.1557/jmr.2018.241.
[39] M. Göbel, A. Rahmel, M. Schütze, The isothermal-oxidation behavior of several nickel-base single-crystal superalloys with and without coatings, Oxidation of Metals 39 (1993) 231-261. https://doi.org/10.1007/BF00665614.
[40] F. Müller, B. Gorr, H.-J. Christ, H. Chen, A. Kauffmann, M. Heilmaier, Effect of Y Additions on the Oxidation Behaviour of Novel Refractory High-Entropy Alloy NbMoCrTiAl at 1000 °C in Air, Oxidation of Metals 94 (2020) 147-163. https://doi.org/10.1007/s11085-020-09983-6.
[41] O.N. Senkov, J.M. Scott, S.V. Senkova, D.B. Miracle, C.F. Woodward, Microstructure and room temperature properties of a high-entropy TaNbHfZrTi alloy, Journal of Alloys and Compounds 509 (2011) 6043-6048. http://dx.doi.org/10.1016/j.jallcom.2011.02.171.
[42] Y.D. Wu, Y.H. Cai, T. Wang, J.J. Si, J. Zhu, Y.D. Wang, X.D. Hui, A refractory Hf25Nb25Ti25Zr25 high-entropy alloy with excellent structural stability and tensile properties, Materials Letters 130 (2014) 277-280.

673 http://dx.doi.org/10.1016/j.matlet.2014.05.134.
674 [43] C.-C. Juan, M.-H. Tsai, C.-W. Tsai, C.-M. Lin, W.-R. Wang, C.-C. Yang, S.-K.
675 Chen, S.-J. Lin, J.-W. Yeh, Enhanced mechanical properties of HfMoTaTiZr and
676 HfMoNbTaTiZr refractory high-entropy alloys, Intermetallics 62 (2015) 76-83.
677 https://doi.org/10.1016/j.intermet.2015.03.013.
678 [44] C.-C. Juan, K.-K. Tseng, W.-L. Hsu, M.-H. Tsai, C.-W. Tsai, C.-M. Lin, S.-K.
679 Chen, S.-J. Lin, J.-W. Yeh, Solution strengthening of ductile refractory
680 HfMoxNbTaTiZr high-entropy alloys, Materials Letters 175 (2016) 284-287.
681 http://dx.doi.org/10.1016/j.matlet.2016.03.133.
682 [45] S. Sheikh, M.K. Bijaksana, A. Motallebzadeh, S. Shafeie, A. Lozinko, L. Gan,
683 T.-K. Tsao, U. Klement, D. Canadinc, H. Murakami, S. Guo, Accelerated oxidation in
684 ductile refractory high-entropy alloys, Intermetallics 97 (2018) 58-66.
685 https://doi.org/10.1016/j.intermet.2018.04.001.
686 [46] S. Sheikh, L. Gan, T.-K. Tsao, H. Murakami, S. Shafeie, S. Guo, Aluminizing for
687 enhanced oxidation resistance of ductile refractory high-entropy alloys, Intermetallics
688 103 (2018) 40-51. https://doi.org/10.1016/j.intermet.2018.10.004.
689 [47] O.N. Senkov, S.V. Senkova, D.M. Dimiduk, C. Woodward, D.B. Miracle,
690 Oxidation behavior of a refractory NbCrMo0.5Ta0.5TiZr alloy, J Mater Sci 47 (2012)
691 6522-6534. https://doi.org/10.1007/s10853-012-6582-0.
692 [48] C.M. Lin, C.C. Juan, C.H. Chang, C.W. Tsai, J.W. Yeh, Effect of Al addition on
693 mechanical properties and microstructure of refractory AlxHfNbTaTiZr alloys,
694 Journal of Alloys and Compounds 624 (2015) 100-107.
695 https://doi.org/10.1016/j.jallcom.2014.11.064.
696 [49] O.N. Senkov, S.V. Senkova, D.B. Miracle, C. Woodward, Mechanical properties
697 of low-density, refractory multi-principal element alloys of the Cr–Nb–Ti–V–Zr
698 system, Materials Science and Engineering: A 565 (2013) 51-62.
699 http://dx.doi.org/10.1016/j.msea.2012.12.018.
700 [50] N. Guo, L. Wang, L. Luo, X. Li, Y. Su, J. Guo, H. Fu, Microstructure and
701 mechanical properties of refractory MoNbHfZrTi high-entropy alloy, Materials &
702 Design 81 (2015) 87-94. https://doi.org/10.1016/j.matdes.2015.05.019.
703 [51] C. Wagner, Reaktionstypen bei der Oxydation von Legierungen, Zeitschrift für
704 Elektrochemie, Berichte der Bunsengesellschaft für physikalische Chemie 63 (1959)
705 772-782. https://doi.org/10.1002/bbpc.19590630713.
706 [52] D. Vojtěch, T. Popela, J. Kubásek, J. Maixner, P. Novák, Comparison of Nb- and
707 Ta-effectiveness for improvement of the cyclic oxidation resistance of TiAl-based
708 intermetallics, Intermetallics 19 (2011) 493-501.
709 https://doi.org/10.1016/j.intermet.2010.11.025.
710 [53] D. Nilsson, N. Stavlid, M. Lindquist, S. Hogmark, U. Wiklund, The role of

711 aluminum additions in the oxidation and wear of a TaC: C low-friction coating,
712 Surface and Coatings Technology 203 (2009) 2989-2994.
713 https://doi.org/10.1016/j.surfcoat.2009.03.008.
714 [54] W. Ren, F. Ouyang, B. Ding, Y. Zhong, J. Yu, Z. Ren, L. Zhou, The influence of
715 CrTaO4 layer on the oxidation behavior of a directionally-solidified nickel-based
716 superalloy at 850–900° C, Journal of Alloys and Compounds 724 (2017) 565-574.
717 https://doi.org/10.1016/j.jallcom.2017.07.066.
718 [55] K.S. Chan, Cyclic oxidation response of multiphase niobium-based alloys,
719 Metallurgical and Materials Transactions A 35 (2004) 589-597.
720 https://doi.org/10.1007/s11661-004-0370-7.
721 [56] S.Y. Qu, Y.F. Han, J.X. Song, Y.W. Kang, Effects of Cr and Al on High
722 Temperature Oxidation Resistance of Nb-Si System Intermetallics, Materials Science
723 Forum 546-549 (2007) 1485-1488.
724 https://doi.org/10.4028/www.scientific.net/MSF.546-549.1485.
725 [57] B. Jasper-Toennies, H. Mueller-Buschbaum, Synthesis and structure of AlTaO4,
726 Zeitschrift fuer Anorganische und Allgemeine Chemie (1950), (1983) 113-116.
727 https://doi.org/10.1002/zaac.19835040914.
728 [58] E.A. Gulbransen, K.F. Andrew, F.A. Brassart, Oxidation of Molybdenum 550° to
729 1700°C, Journal of The Electrochemical Society 110 (1963) 952-959.
730 https://doi.org/10.1149/1.2425918.
731 [59] Y. Shida, H. Anada, The effect of various ternary additives on the oxidation
732 behavior of TiAl in high-temperature air, Oxidation of Metals 45 (1996) 197-219.
733 https://doi.org/10.1007/BF01046826.
734 [60] P. Pérez, J.A. Jiménez, G. Frommeyer, P. Adeva, Oxidation behaviour of a
735 Ti–46Al–1Mo–0.2Si alloy: the effect of Mo addition and alloy microstructure,
736 Materials Science and Engineering: A 284 (2000) 138-147.
737 https://doi.org/10.1016/S0921-5093(00)00755-3.
738 [61] O.N. Senkov, J.M. Scott, S.V. Senkova, F. Meisenkothen, D.B. Miracle, C.F.
739 Woodward, Microstructure and elevated temperature properties of a refractory
740 TaNbHfZrTi alloy, J Mater Sci 47 (2012) 4062-4074.
741 https://doi.org/10.1007/s10853-012-6260-2.
742 [62] R.N. Patil, E.C. Subbarao, Axial thermal expansion of ZrO2 and HfO2 in the
743 range room temperature to 1400°C, Journal of Applied Crystallography 2 (1969)
744 281-288. https://doi.org/10.1107/S0021889869007217.
745 [63] M. Yoshihara, Influence of Zr Addition on Oxidation Behavior of TiAl-Based
746 Alloys, Materials Science Forum 696 (2011) 360-365.
747 https://doi.org/10.4028/www.scientific.net/MSF.696.360.
748 [64] R.E. Newnham, Crystal Structure of ZrTiO4, Journal of the American Ceramic

749 Society 50 (1967) 216-216. https://doi.org/10.1111/j.1151-2916.1967.tb15085.x.
750 [65] D.-C. Tsai, Z.-C. Chang, L.-Y. Kuo, T.-J. Lin, T.-N. Lin, M.-H. Shiao, F.-S. Shieu,
751 Oxidation resistance and structural evolution of (TiVCrZrHf)N coatings, Thin Solid
752 Films 544 (2013) 580-587. https://doi.org/10.1016/j.tsf.2012.12.064.
753 [66] E.B. Kashkarov, M.S. Syrtanov, A.E. Shevelev, A.V. Kurochkin, S.K. Pavlov,
754 High-temperature oxidation resistance of Ti-implanted E110 alloy, IOP Conference
755 Series: Materials Science and Engineering 597 (2019), 012059.
756 https://doi.org/10.1088/1757-899x/597/1/012059.
757 [67] B. Gorr, S. Schellert, F. Müller, H.-J. Christ, A. Kauffmann, M. Heilmaier,
758 Current Status of Research on the Oxidation Behavior of Refractory High Entropy
759 Alloys, Advanced Engineering Materials 23 (2021), 2001047.
760 https://doi.org/10.1002/adem.202001047.
761 [68] B.A. Pint, J.R. DiStefano, The Role of Oxygen Uptake and Scale Formation on
762 the Embrittlement of Vanadium Alloys, Oxidation of Metals 63 (2005) 33-55.
763 https://doi.org/10.1007/s11085-005-1950-7.
764 [69] D. Feng, J. Zhang, M. Li, M. Chen, B. Zhao, Phase Equilibria of the SiO2–V2O5
765 system, Ceramics International 46 (2020) 24053-24059.
766 https://doi.org/10.1016/j.ceramint.2020.06.183.
767 [70] H. Schadow, H. Oppermann, B. Wehner, Investigations on the Quasi-binary
768 System V2O5-Ta2O5, Crystal Research and Technology 27 (1992) 691-695.
769 https://doi.org/10.1002/crat.2170270520.
770 [71] G. Chen, Z. Sun, X. Zhou, Oxidation of Intermetallic Alloys in Ti-Al-Nb Ternary
771 System, CORROSION 48 (1992) 939-946. https://doi.org/10.5006/1.3315897.
772 [72] M. Yoshihara, K. Miura, Effects of Nb addition on oxidation behavior of TiAl,
773 Intermetallics 3 (1995) 357-363. https://doi.org/10.1016/0966-9795(95)94254-C.
774 [73] J. Chen, Q. Chen, S.J. Qu, H.P. Xiang, C. Wang, J.B. Gao, A.H. Feng, D.L. Chen,
775 Oxidation mechanisms of an intermetallic alloy at high temperatures, Scripta
776 Materialia 199 (2021), 113852. https://doi.org/10.1016/j.scriptamat.2021.113852.
777 [74] Z. Hong, H. Zhang, J.-F. Weng, L.-F. Su, Z. Li, L.-N. Jia, Oxidation behavior of
778 Nb–24Ti–18Si–2Al–2Hf–4Cr and Nb–24Ti–18Si–2Al–2Hf–8Cr hypereutectic alloys
779 at 1250 °C, Rare Metals 36 (2017) 168-173.
780 https://doi.org/10.1007/s12598-015-0600-8.
781 [75] J.A. Ventura, B.I. Portillo, S.K. Varma, R.N. Mahapatra, Oxidation Behavior of
782 Nb-20Mo-15Si-5B-20Cr and Nb-20Mo-15Si-5B-20Ti Alloys Up To 1300°C, ECS
783 Transactions 16 (2019) 157-166. https://doi.org/10.1149/1.3224752.
784 [76] B. Portillo, P. Kakarlapudi, S.K. Varma, The possible application of Nb-W-Cr
785 alloys in high-temperature air, JOM 59 (2007) 46-49.
786 https://doi.org/10.1007/s11837-007-0078-4.

787